Breaking Scaling Relations and Boosting Ammonia Synthesis in Nitrogen Reduction with V-Containing Heteronuclear Double Metal Atoms

Bingling He[1,2], Mingyang Ren[4], Liying Zhang[2], Peng Lv[5,6*], Mengyin Liu[1], Song Ye[1] and Yu Jia[2,3*]

[1]*School of Electronic Engineering, Chaohu University, Hefei 238000, China*
[2]*Key Laboratory for Special Functional Materials of Ministry of Education, and School of Materials Science and Engineering, Henan University, Kaifeng, 475001, China*
[3]*International Laboratory for Quantum Functional Materials of Henan, and School of Physics and Engineering, Zhengzhou University, Zhengzhou 450001, China*
[4]*College of Physics and Electronic Information Engineering, Guilin University of Technology, Guilin, 541004, China*
[5] *Key Laboratory for High Efficiency Energy Conversion Science and Technology of Henan Province, International Joint Research Laboratory of New Energy Materials and Devices of Henan Province, School of Physics and Electronics, Henan University, Kaifeng, 475004, P. R. China*
[6]*Guangdong Provincial Key Laboratory of Electronic Functional Materials and Devices, Huizhou University, Huizhou 516001, China*

Supporting Information

* Corresponding author. E-mail: lvpeng@henu.edu.cn (Peng Lv)
* Corresponding author. E-mail: jiayu@henu.edu.cn (Yu Jia)

Note S1 Calculations of formation energy (E_f) and the dissolution potential (U_{diss}) for V-TM@GDY.

The thermodynamic stability and electrochemical stability were evaluated by the formation energy (E_f) and the dissolution potential (U_{diss}), defined as:[1]

$$E_f = E(total) - E(GDY) - E(V\text{-}bulk) - E(TM\text{-}bulk)$$

$$U_{diss} = U^0 - E_f/ne$$

Where E(total) and E(GDY) are the total energies of GDY with and without the V-TM pairs, respectively, and E(V-bulk) and E(TM-bulk) are the energies of the V and TM atoms in their bulk, respectively. U^0 denotes the standard dissolution potential of bulk TM, and n is the number of electrons involved in the dissolution. The values of U^0 and n comes from the previous literature.[1]

Note S2 Calculations of binding energy (E_b) between the V-TM pairs and GDY

The binding energy (E_b) was calculated to estimate the binding ability, which is defined as:

$$E_b = E(total) - E(GDY) - E(V\text{-}atom) - E(TM\text{-}atom)$$

Here, E(total) and E(GDY) represent the total energies of the GDY monolayer with and without the anchored atoms, respectively. E(V-atom) and E(TM-atom) are the energies of the V and TM atoms in vacuum, respectively. The more negative E_b represents a larger binding strength.

Note S3 Calculations of the adsorption free energy for the absorbates.

The adsorption free energy, $\Delta G(X)$, was calculated using the equation:

$$\Delta G(X) = G(sub+X) - G(sub) - G(X)$$

where G(sub+X) and G(sub) are the free energies of the systems with and without the adsorbate, respectively, and G(X) is the free energy of the X molecule in vacuum.

Note S4 Calculations of theoretical Faradaic efficiency (FE)

HER is a major competing reaction to NRR. The catalytic selectivity based on theoretical FE can be estimated using the Boltzmann distribution[2] and is calculated using the following formula:[3-4]

$$\mathrm{FE} = \frac{1}{1 + e^{-\frac{\delta G}{k_B T}}} \times 100\%$$

where δG represents the difference in Gibbs free energy change of the PDS between HER and NRR, k_B is the Boltzmann constant, and T = 298.15 K. This formula is based on two assumptions: (1) only HER and NRR are considered as competing side reactions, and (2) proton and electron transfer are not the rate-determining steps for either HER or NRR.

Table S1 Zero-point energy corrections (ΔE_{ZPE}, eV), and entropic contributions (at 298.15 K) to the free energies ($T\Delta S$, eV). The values for the free molecules were obtained from Ref. 5.

Species	**ΔE_{ZPE} (eV)**	**$T\Delta S$ (eV)**
N_2	0.15	0.58
*N-*N	0.21	0.09
*N-*NH	0.52	0.09
N-NH_2	0.86	0.11
*NH-*NH	0.81	0.12
NH-NH_2	1.15	0.15
NH_2-NH_2	1.51	0.16
*N	0.09	0.04
*NH	0.36	0.07
*NH_2	0.69	0.08
*NH_3	1.03	0.15
NH_3	0.89	0.60
H_2O	0.56	0.67
*H_2O	0.66	0.14
*H	0.16	0.02

Table S2 Binding energy (E_b, eV), formation energy (E_f, eV), dissolution potential (U_{diss}, V), bond length between V and the TM ($d_{V\text{-}TM}$, Å), number of transferred electrons to V (Qv, *e*) and TM (Q_{TM}, *e*) for V-TM@GDY, and d band center of V (ε_d(V), eV) and TM (ε_d(TM), eV) atoms.

System	E_b	E_f	U_{diss}	$d_{V\text{-}TM}$	Q_V	Q_{TM}	ε_d(V)	ε_d(TM)
V-Sc	-8.98	1.62	-1.95	2.68	-0.89	-1.39	-0.01	0.47
V-Ti	-9.11	2.90	-2.13	2.70	-0.90	-1.17	-0.01	-0.02
V-V	-7.99	3.78	-2.12	2.64	-0.95	-0.95	-0.21	-0.22
V-Cr	-6.62	3.68	-1.96	2.57	-0.96	-0.83	-0.24	-0.20
V-Mn	-6.78	3.14	-1.97	2.59	-0.97	-0.68	-0.26	-0.86
V-Fe	-8.09	3.22	-1.62	2.35	-0.99	-0.45	-0.30	-1.42
V-Co	-8.45	3.08	-1.50	2.34	-1.02	-0.25	-0.23	-1.32
V-Ni	-8.12	2.94	-1.45	2.41	-1.00	-0.23	-0.20	-1.98
V-Cu	-3.84	3.86	-1.39	2.60	-0.97	-0.30	0.02	-3.33

Table S3 N_2 adsorption free energy ($\Delta G(N_2)$, eV), N-N bond length (d_{N-N}, Å), number of transferred electrons to N_2 ($\Delta Q(N_2)$, *e*), N-N ICOHP for the adsorbed N_2 molecules ($ICOHP(N_2)$), potential-determining step (PDS), and limiting potential ($U_L(NH_3)$, in V) for NRR on V-TM@GDY.

System	$\Delta G(N_2)$	d_{N-N}	$\Delta Q(N_2)$	$ICOHP(N_2)$	PDS	$U_L(NH_3)$
V-Sc-side	-0.88	1.20	0.77	-9.27	$*NH_2 + H^+ + e^- \rightarrow *NH_3$	-0.99
V-Ti-side	-1.32	1.21	0.76	-9.01	$*NH_2 + H^+ + e^- \rightarrow *NH_3$	-0.87
V-V-side	-1.34	1.23	0.85	-8.46	$*NH_2 + H^+ + e^- \rightarrow *NH_3$	-0.74
V-Cr-side	-1.00	1.21	0.74	-9.18	$*NH_2 + H^+ + e^- \rightarrow *NH_3$	-0.36
V-Mn-side	-0.62	1.18	0.61	-9.81	$*NH_2 + H^+ + e^- \rightarrow *NH_3$	-0.41
V-Fe-side	-0.69	1.19	0.59	-9.73	$*NH_2 + H^+ + e^- \rightarrow *NH_3$	-0.42
V-Co-side	-0.63	1.18	0.59	-9.70	$*NH_2 + H^+ + e^- \rightarrow *NH_3$	-0.63
V-Ni-side	-0.36	1.17	0.52	-10.02	$*NH_2 + H^+ + e^- \rightarrow *NH_3$	-0.71
V-Cu-side	-0.40	1.19	0.62	-9.52	$*NH_2 + H^+ + e^- \rightarrow *NH_3$	-0.42
V-Cr-end	-0.16	1.13	0.25	-11.09	/	/
V-Mn-end	-0.26	1.14	0.36	-10.71	/	/
V-Fe-end	-0.66	1.14	0.37	-10.63	$*NN + H^+ + e^- \rightarrow *NNH$	-0.50
V-Co-end	-0.67	1.14	0.35	-10.62	$*NH_2 + H^+ + e^- \rightarrow *NH_3$	-0.63
V-Ni-end	-0.41	1.15	0.38	-10.35	$*NH_2 + H^+ + e^- \rightarrow *NH_3$	-0.71
V-Cu-end	-0.59	1.14	0.26	-10.98	$*NN + H^+ + e^- \rightarrow *NNH$	-0.53

Table S4 Adsorption free energy of NH_2 ($\Delta G(NH_2)$, eV), NH_3 ($\Delta G(NH_3)$, eV), H ($\Delta G(H)$, eV), and H_2O ($\Delta G(H_2O)$, eV), desorption energy of NH_3 ($\Delta G_{des}(NH_3)$, eV), and Faradaic efficiency (FE) of NRR.

System	$\Delta G(NH_2)$	$\Delta G(NH_3)$	$\Delta G_{des}(NH_3)$	$\Delta G(H)$	FE	$\Delta G(H_2O)$
V-Sc	-2.51	-1.52	0.79	-0.54	0%	-0.48
V-Ti	-2.63	-1.76	1.03	-0.61	0%	-0.57
V-V	-2.67	-1.93	1.20	-0.19	0%	-0.73
V-Cr	-2.25	-1.88	1.15	-0.76	100%	-0.59
V-Mn	-2.34	-1.93	1.20	-0.68	100%	-0.40
V-Fe	-2.24	-1.82	1.08	-0.67	99.99%	-0.60
V-Co	-2.36	-1.73	0.99	-0.79	99.81%	-0.68
V-Ni	-2.46	-1.75	1.02	-0.86	99.72%	-0.56
V-Cu	-2.43	-2.01	1.28	-1.01	100%	-0.61

Table S5 Number of electrons transferred to V-Cr (Q(V-Cr), *e*), V-Fe (Q(V-Fe), *e*), N_xH_y (Q(N_xH_y), *e*), and GDY (Q(GDY), *e*) during the NRR processes on V-Cr@GDY and V-Fe@GDY, respectively.

V-Cr	Q(V-Cr)	Q(N_xH_y)	Q(GDY)	V-Fe	Q(V-Fe)	Q(N_xH_y)	Q(GDY)
*+N_2	-1.79	0.00	1.79	*+N_2	-1.46	0.00	1.46
*N-*N	-2.28	0.74	1.55	*N-*N	-1.88	0.58	1.29
*N-*NH	-2.36	0.77	1.59	*N-*NH	-2.01	0.70	1.31
*NH-*NH	-2.29	0.70	1.59	*NH-*NH	-2.05	0.59	1.46
NH-NH_2	-2.20	0.34	1.86	*NH-*NH_2	-1.93	0.28	1.65
*NH	-2.32	0.78	1.54	*NH	-1.92	0.69	1.23
*NH_2	-2.17	0.42	1.76	*NH_2	-1.83	0.39	1.45
*NH_3	-1.97	-0.15	2.12	*NH_3	-1.62	-0.15	1.77

Table S6 The potential-determining step (PDS) and limiting potential ($U_L(NH_3)$, in V) for V-TM@GDY in our work, compared with those for TM@GDY from reference[6].

System	PDS	$U_L(NH_3)$	system	PDS	$U_L(NH_3)$
V-Sc	$*NH_2 + H^+ + e^- \rightarrow *NH_3$	-0.99	Sc@GDY	$*N_2 + H^+ + e^- \rightarrow *NNH$	-1.41
V-Ti	$*NH_2 + H^+ + e^- \rightarrow *NH_3$	-0.87	Ti@GDY	$*N_2 + H^+ + e^- \rightarrow *NNH$	-0.87
V-V	$*NH_2 + H^+ + e^- \rightarrow *NH_3$	-0.74	V@GDY	$*N_2 + H^+ + e^- \rightarrow *NNH$	-0.67
V-Cr	$*NH_2 + H^+ + e^- \rightarrow *NH_3$	-0.36	Cr@GDY	---	---
V-Mn	$*NH_2 + H^+ + e^- \rightarrow *NH_3$	-0.41	Mn@GDY	$*N_2 + H^+ + e^- \rightarrow *NNH$	-1.00
V-Fe	$*NH_2 + H^+ + e^- \rightarrow *NH_3$	-0.42	Fe@GDY	$*N_2 + H^+ + e^- \rightarrow *NNH$	-0.74
V-Co	$*NH_2 + H^+ + e^- \rightarrow *NH_3$	-0.63	Co@GDY	$*N_2 + H^+ + e^- \rightarrow *NNH$	-0.78
V-Ni	$*NH_2 + H^+ + e^- \rightarrow *NH_3$	-0.71	Ni@GDY	$*N_2 + H^+ + e^- \rightarrow *NNH$	-1.75
V-Cu	$*NH_2 + H^+ + e^- \rightarrow *NH_3$	-0.42	Cu@GDY	$*N_2 + H^+ + e^- \rightarrow *NNH$	-1.69

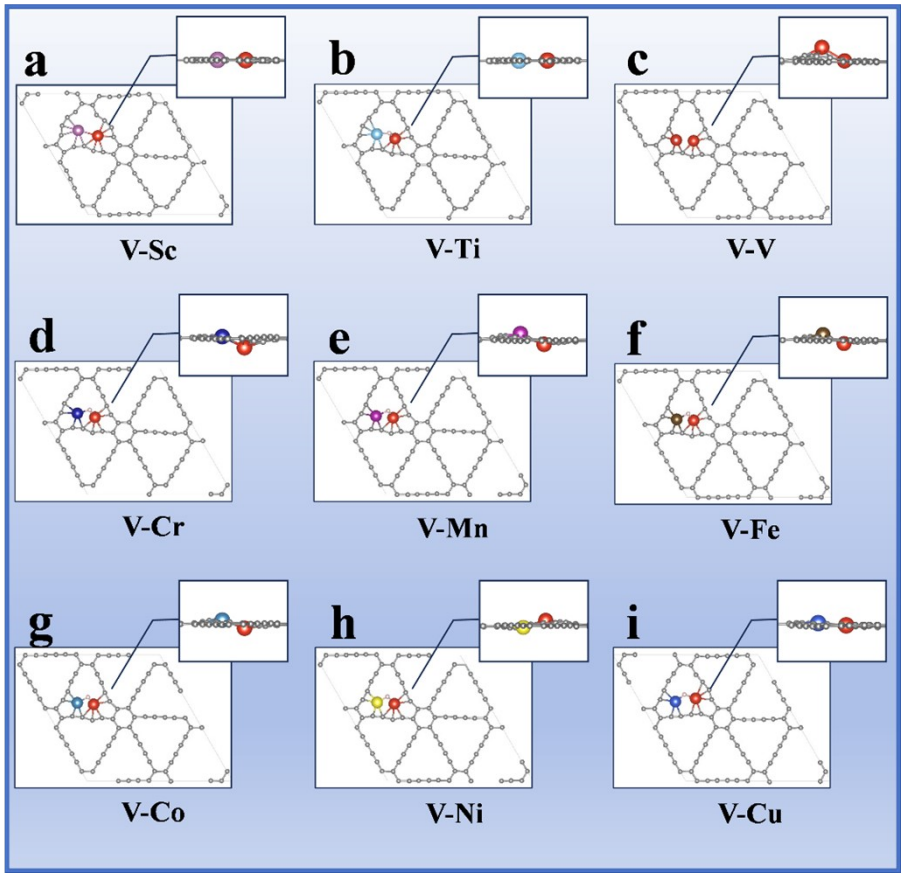

Fig. S1 Optimized structures of V-Sc@GDY (a), V-Ti@GDY (b), V-V@GDY (c), V-Cr@GDY (d), V-Mn@GDY (e), V-Fe@GDY (f), V-Co@GDY (g), V-Ni@GDY (h), and V-Cu@GDY (i).

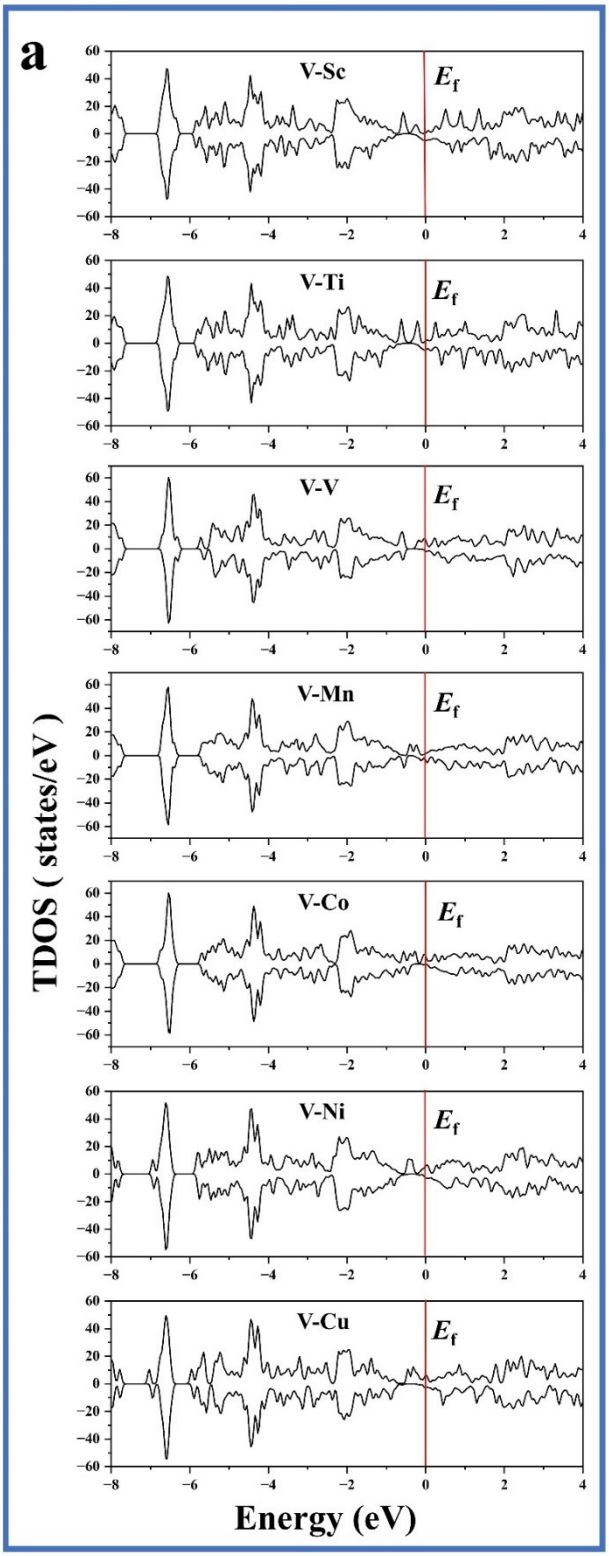
a
V-Sc
V-Ti
V-V
V-Mn
V-Co
V-Ni
V-Cu
E_f
TDOS (states/eV)
Energy (eV)

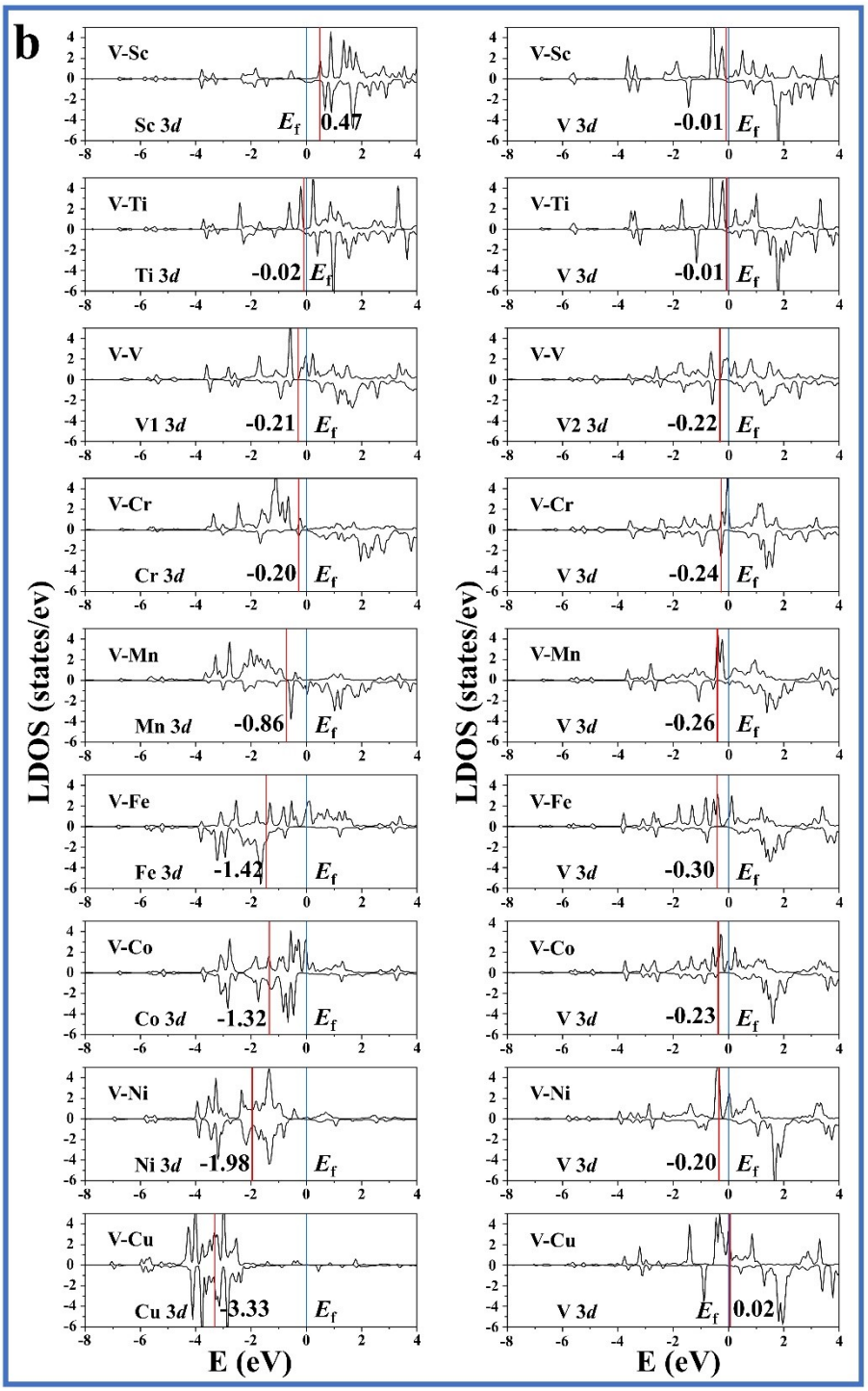

Fig. S2 The TDOS (a) and LDOS (b) for the V-TM@GDY (TM = Sc ~ Cu).

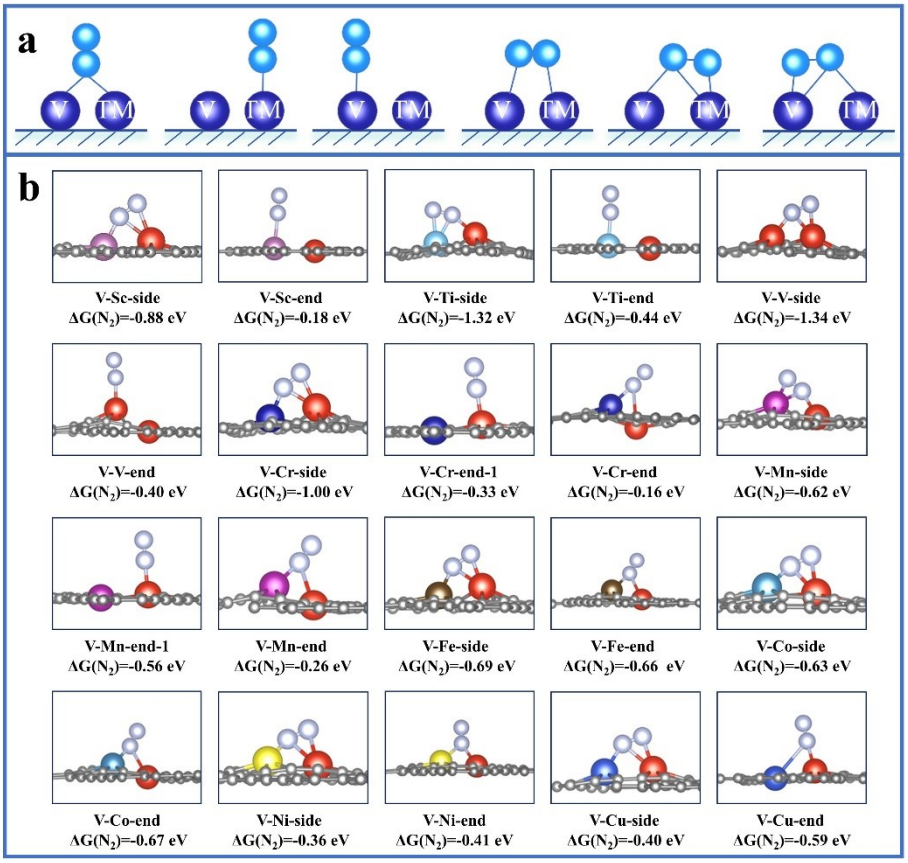

Fig. S3 The considered N_2 adsorption configuration (a), and most stable N_2 side-on and end-on configurations on V-TM@GDY (Sc = Sc to V).

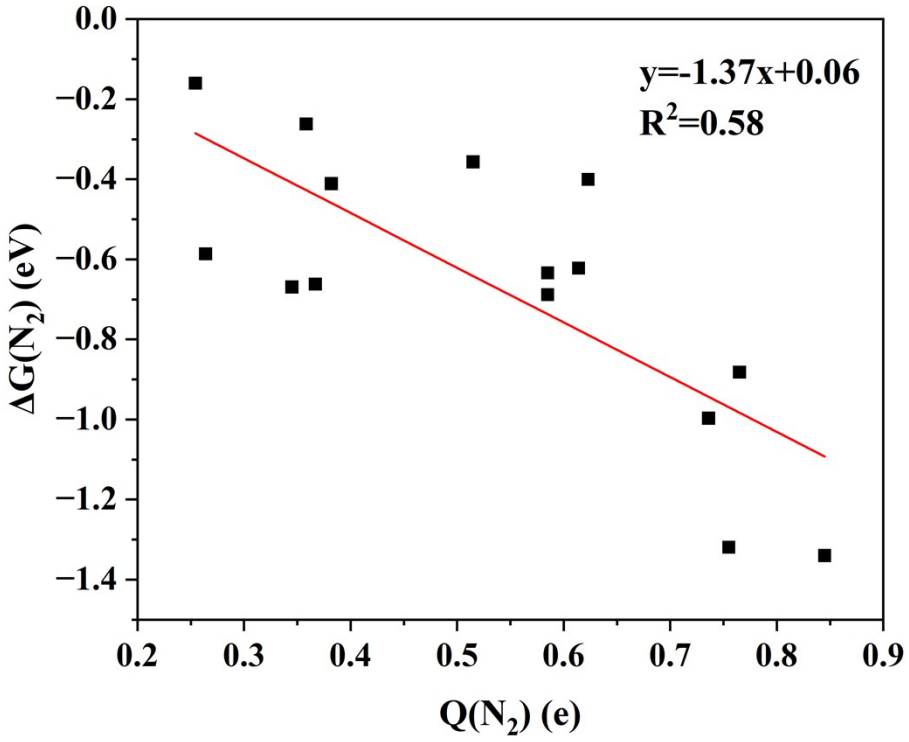

Fig. S4 The N_2 adsorption free energy ($\Delta G(N_2)$) versus the corresponding number of transferred electrons on N_2 ($Q(N_2)$). A positive $Q(N_2)$ value indicates that the N_2 molecules have gained electrons.

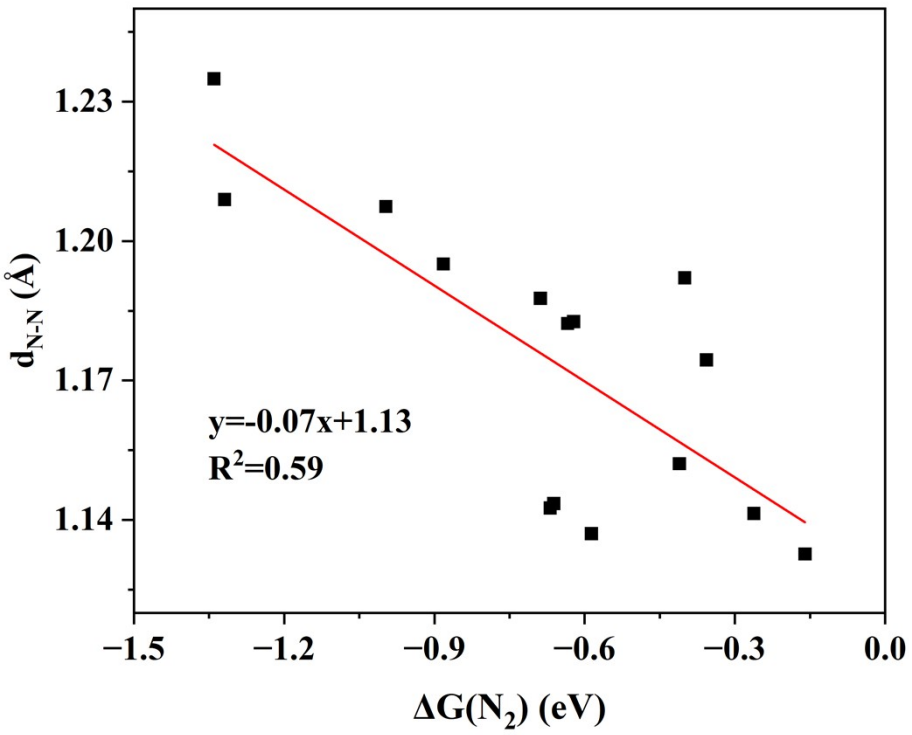

Fig. S5 The N-N bond length (d_{N-N}) versus the corresponding N_2 adsorption free energy ($\Delta G(N_2)$).

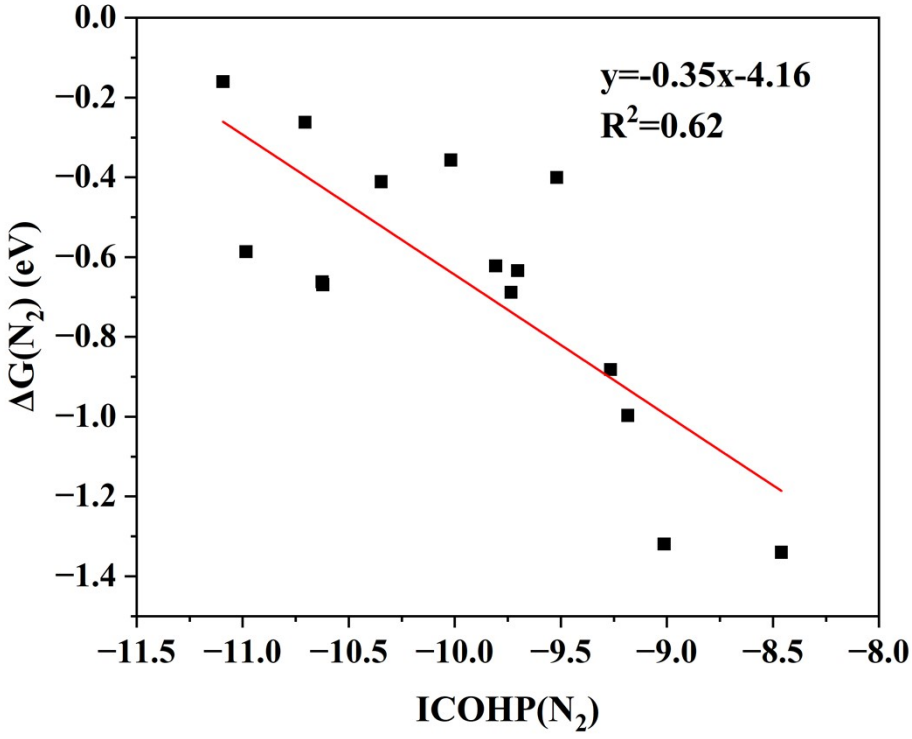

Fig. S6 The N_2 adsorption free energy ($\Delta G(N_2)$) versus the ICOHP of N-N bond (ICOHP(N_2)).

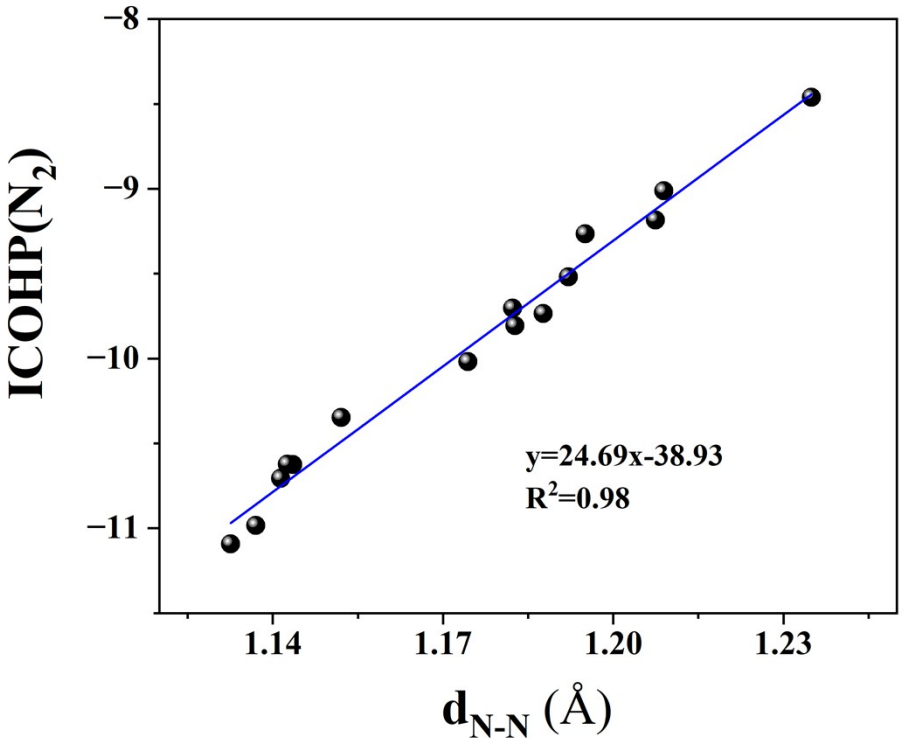

Fig. S7 The ICOHP of N-N bond (ICOHP(N_2)) versus the N-N bond length (d_{N-N}).

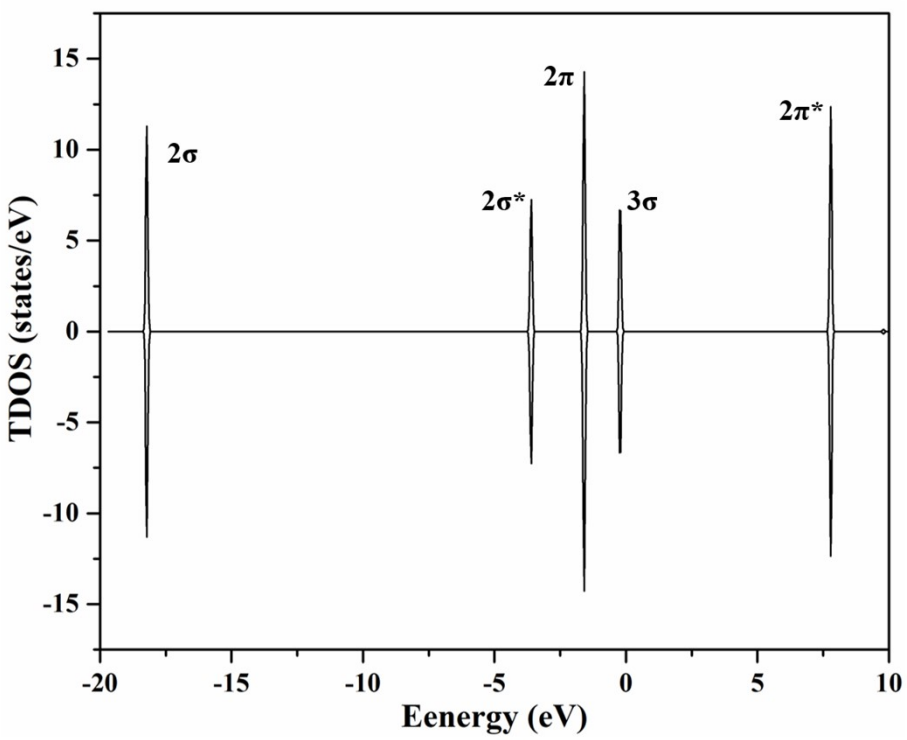

Fig. S8 Total density of states for free N_2 molecule.

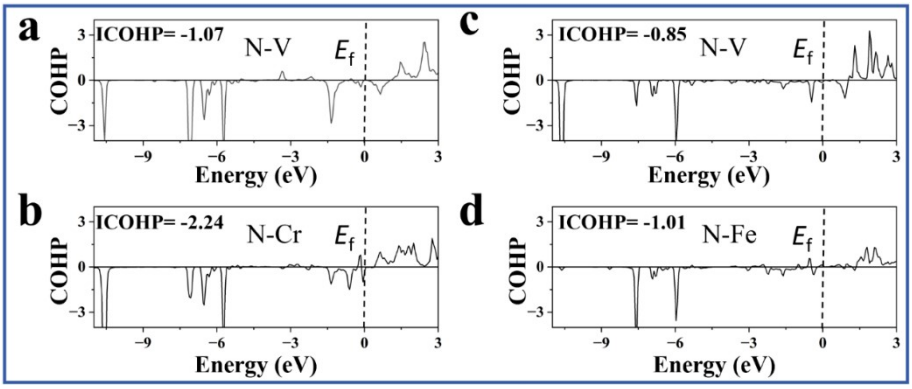

Fig. S9 COHP for the interactions between N of adsorbed N_2 and its bonded V and Cr atoms for N_2 adsorbed V-Cr@GDY (a-b), and V and Fe for N_2 adsorbed V-Fe@GDY (c-d).

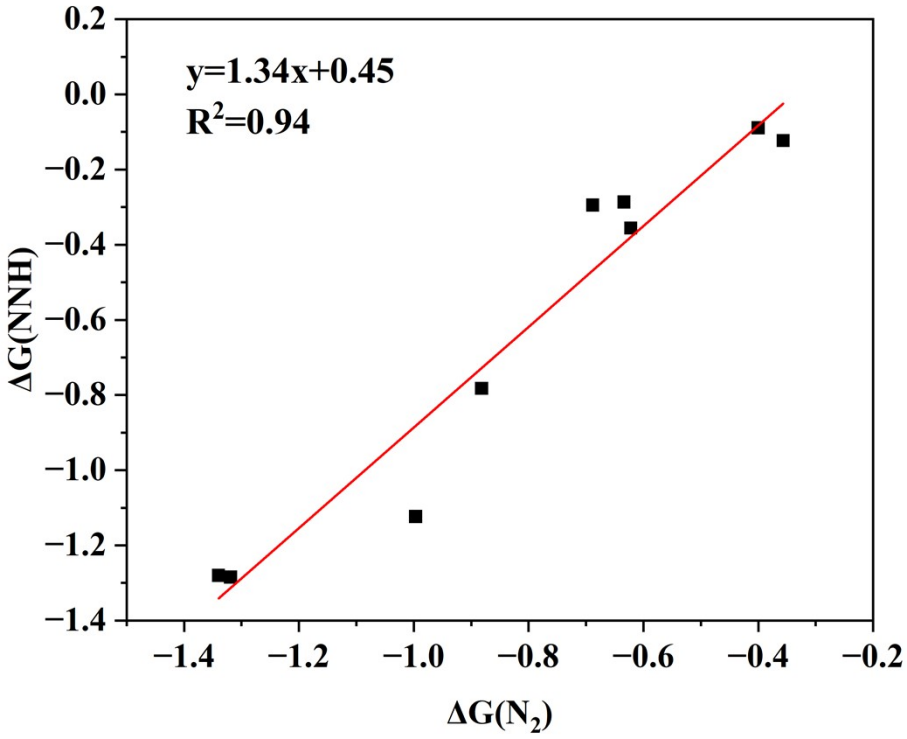

Fig. S10 The NNH adsorption free energy (ΔG(NNH)) versus the corresponding N_2 adsorption free energy (ΔG(N_2)).

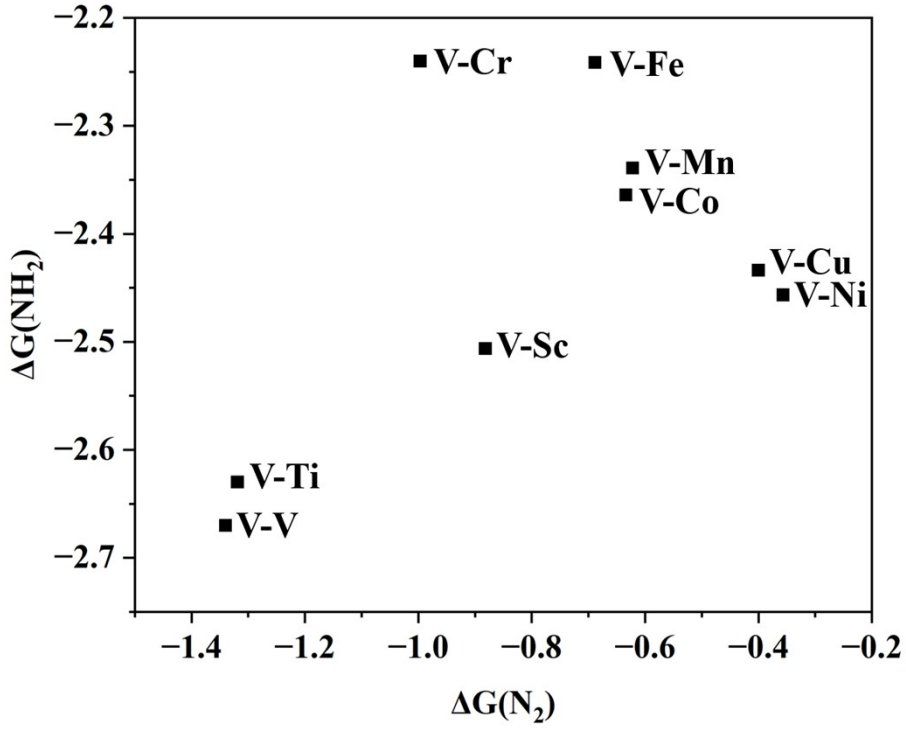

Fig. S11 The NH_2 adsorption free energy ($\Delta G(NH_2)$) versus the corresponding N_2 adsorption free energy ($\Delta G(N_2)$).

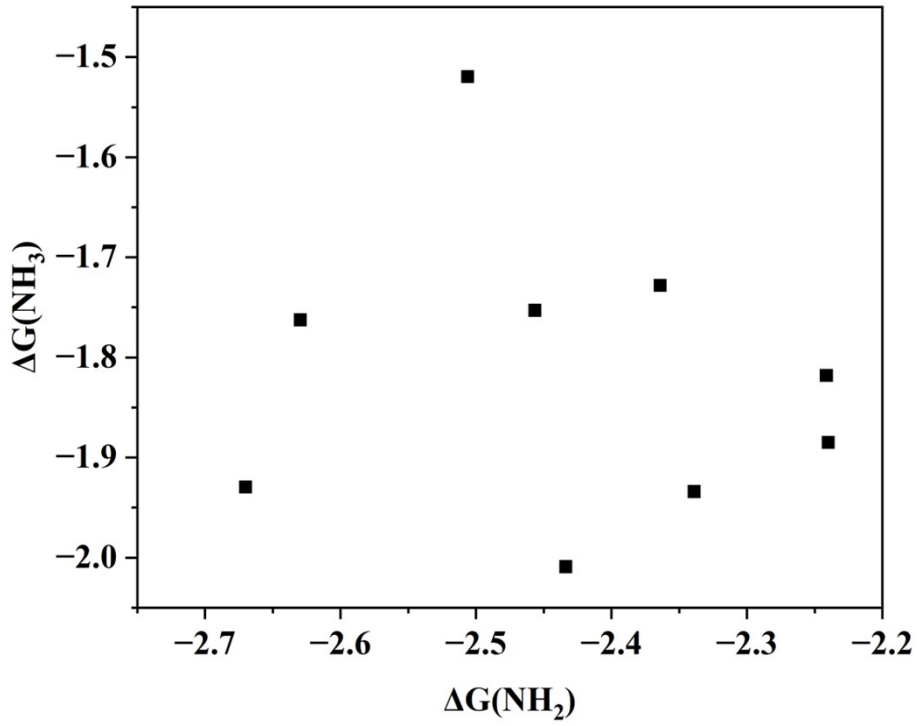

Fig. S12 The NH_3 adsorption free energy ($\Delta G(NH_3)$) versus the corresponding NH_2 adsorption free energy ($\Delta G(NH_2)$).

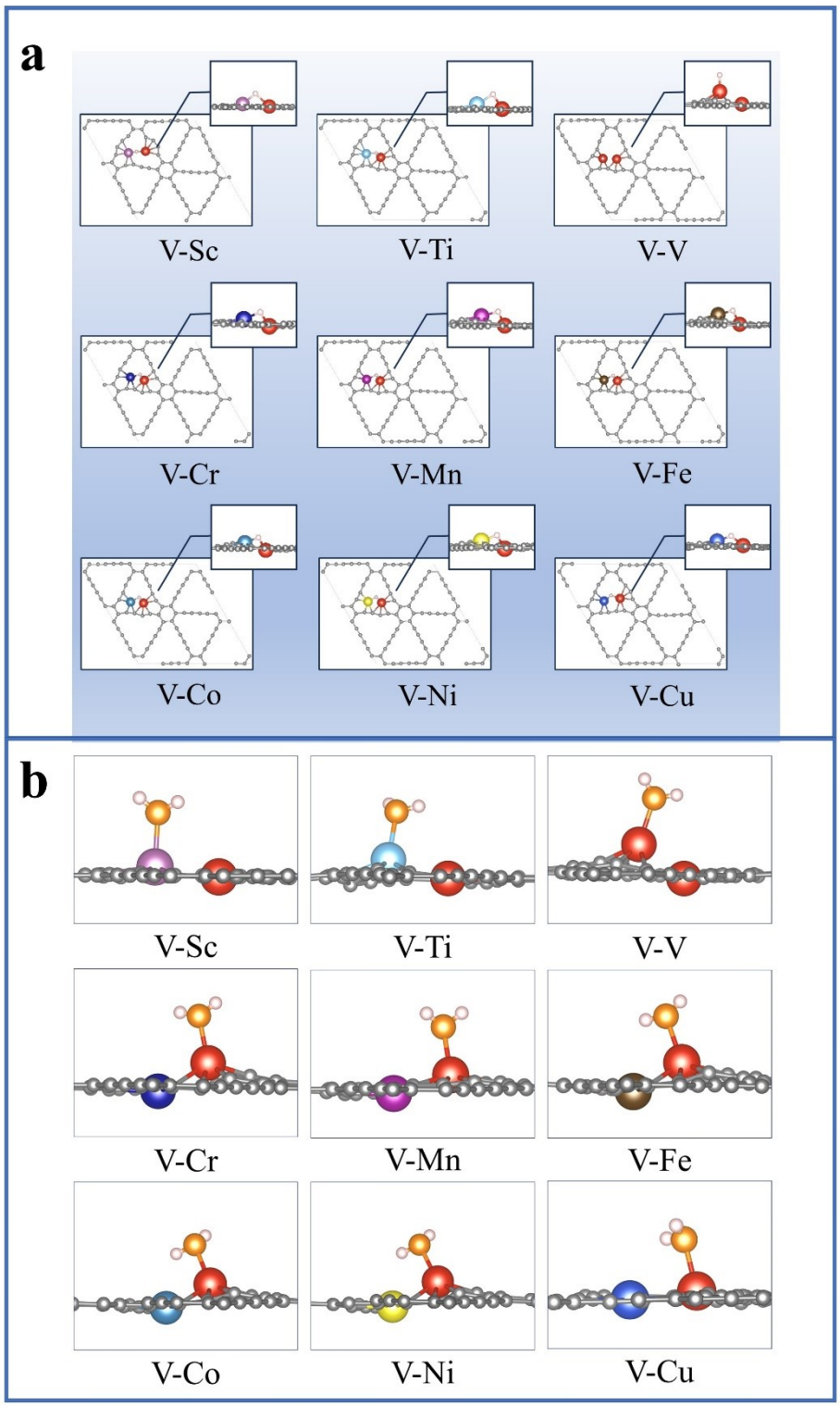

Fig. S13 Optimized H (a) and H_2O (b) adsorption configurations on V-TM@GDY (TM = Sc to Cu).

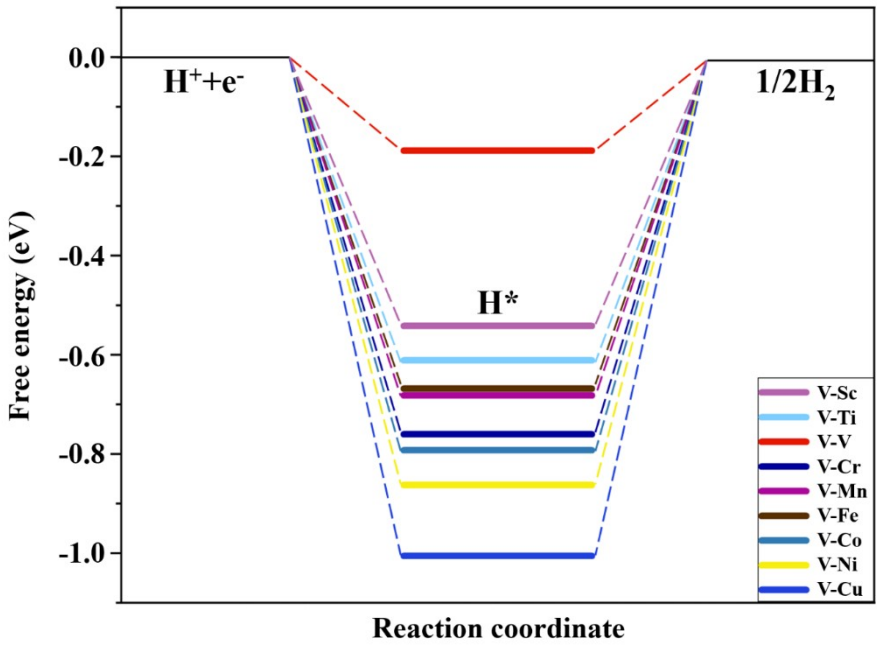

Fig. S14 Free energy diagram of HER for V-TM@GDY.

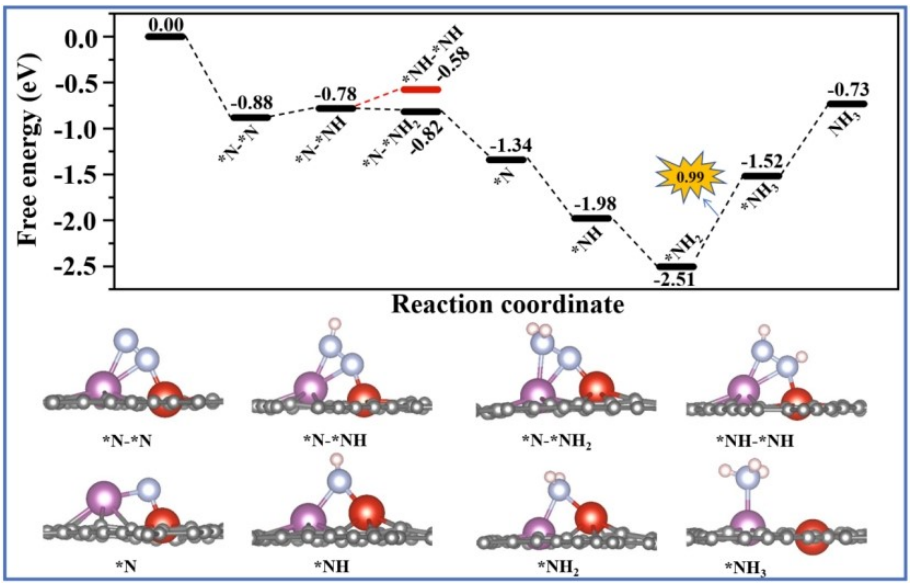

Fig. S15 Free energy diagrams and corresponding reaction intermediates for NRR via a consecutive pathway on V-Sc@GDY.

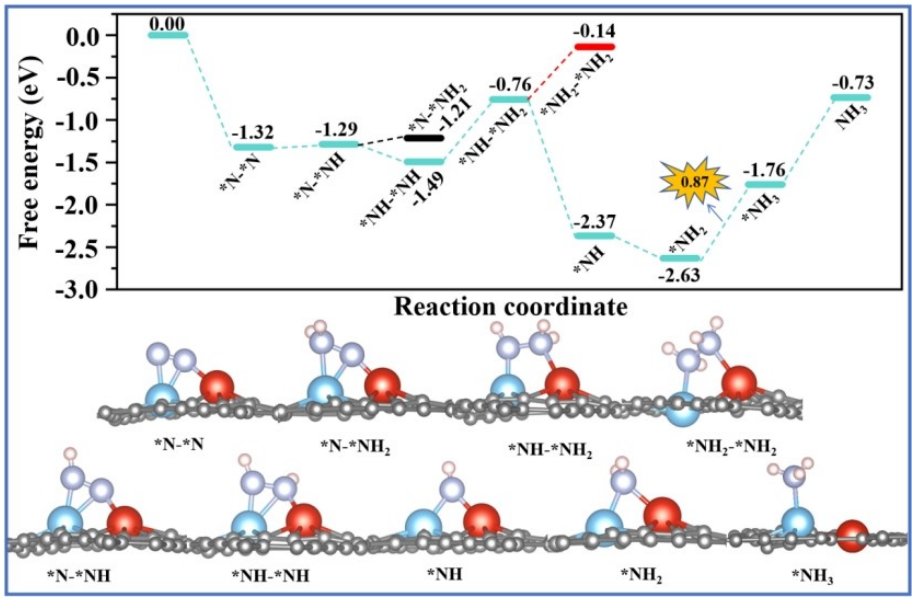

Fig. S16 Free energy diagrams and corresponding reaction intermediates for NRR via a mixed pathway on V-Ti@GDY.

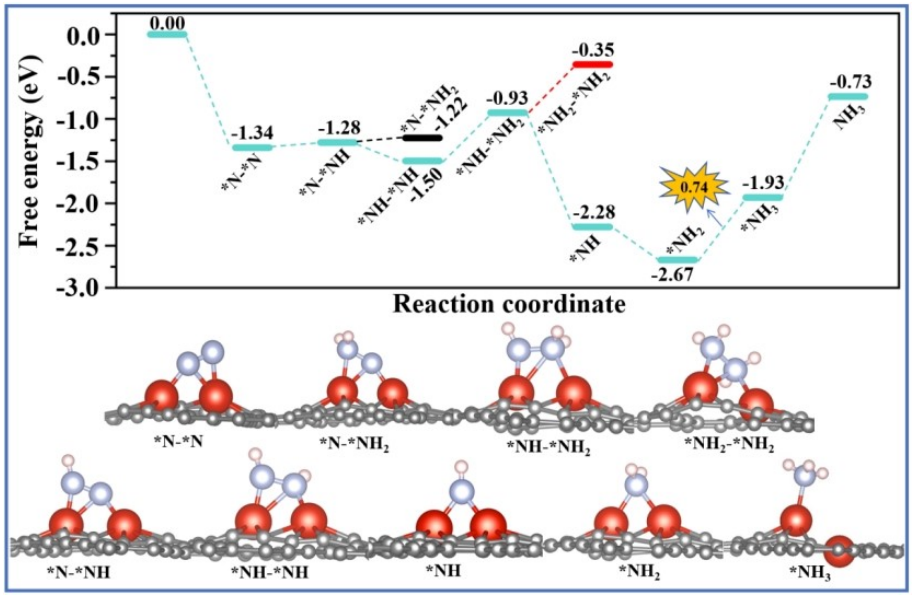

Fig. S17 Free energy diagrams and corresponding reaction intermediates for NRR via a mixed pathway on V-V@GDY.

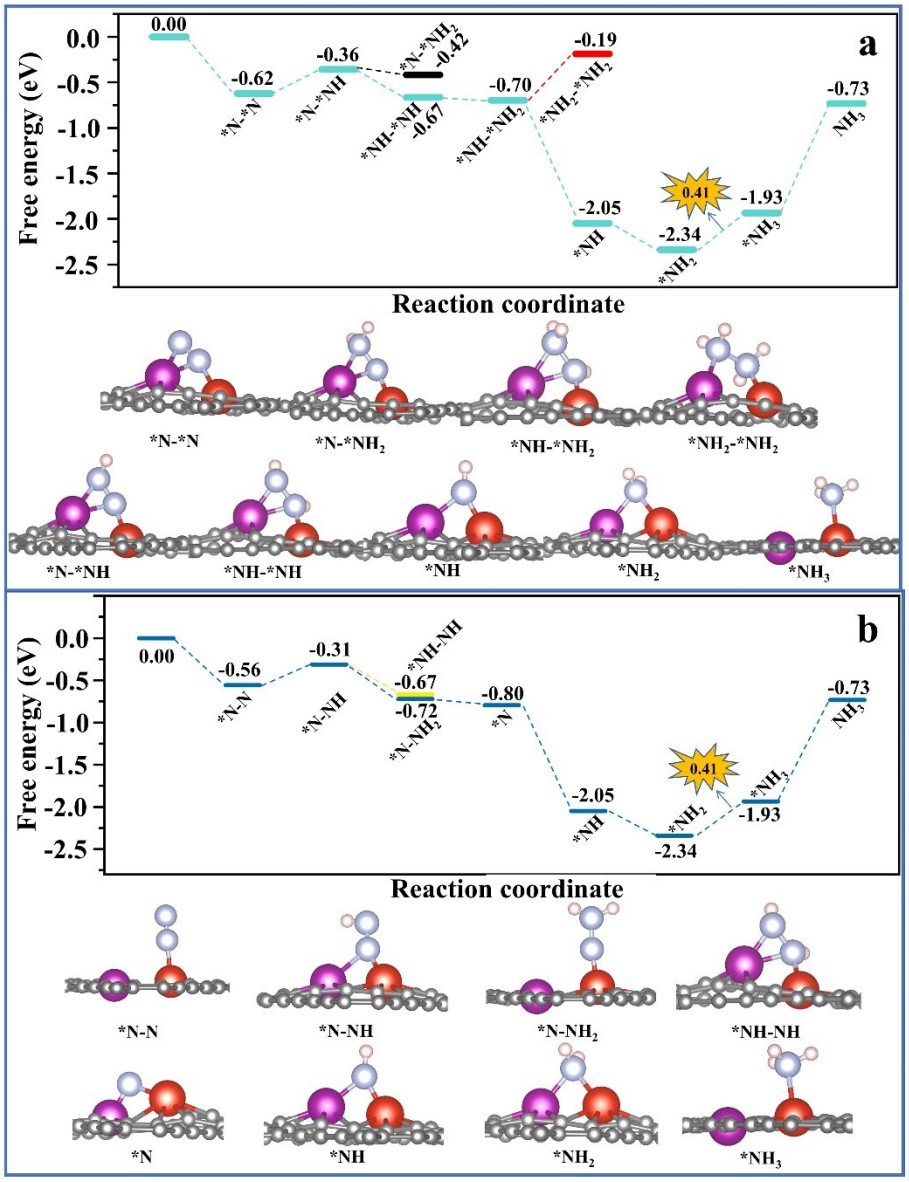

Fig. S18 Free energy diagrams and corresponding reaction intermediates for NRR via a mixed pathway on V-Mn@GDY(a) and distal pathway (b).

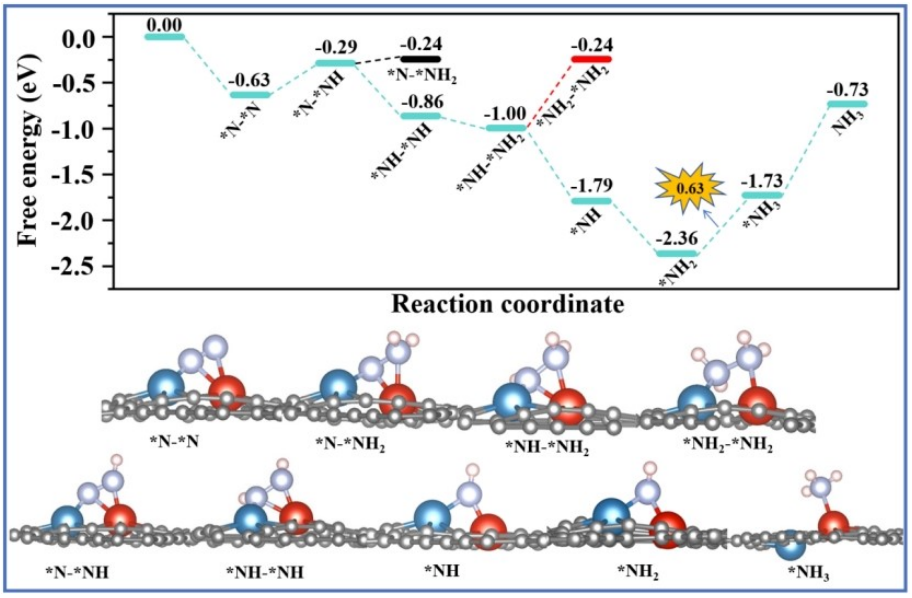

Fig. S19 Free energy diagrams and corresponding reaction intermediates for NRR via a mixed pathway on V-Co@GDY.

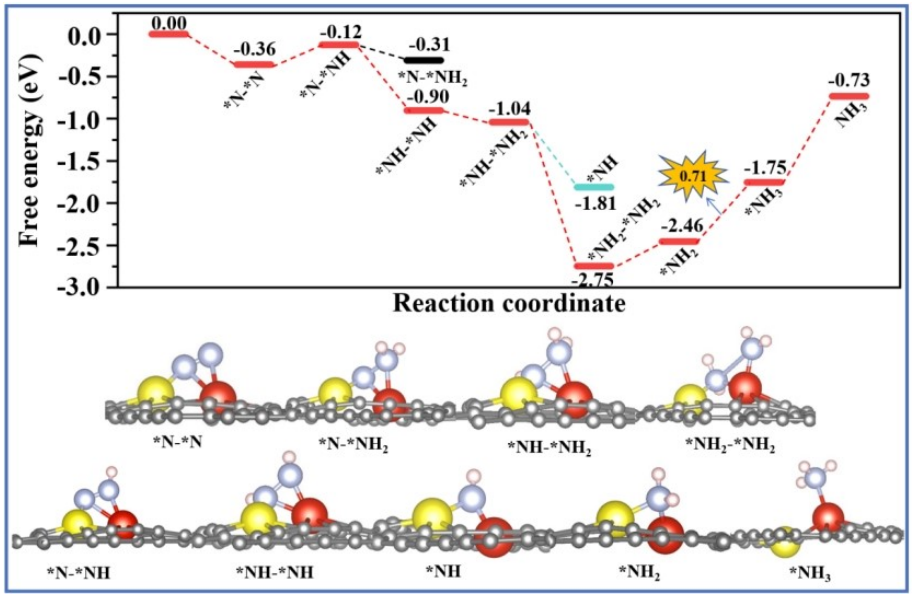

Fig. S20 Free energy diagrams and corresponding reaction intermediates for NRR via an enzymatic pathway on V-Ni@GDY.

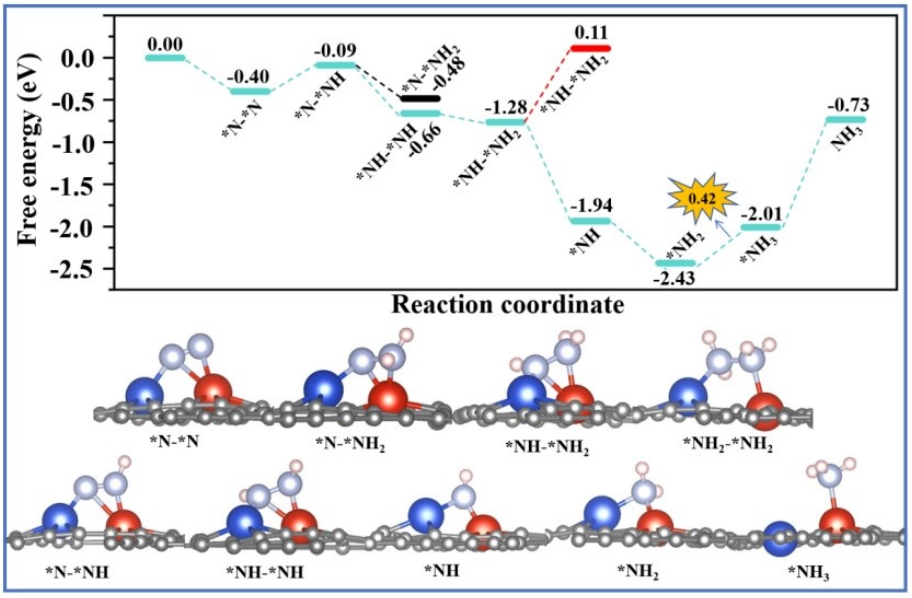

Fig. S21 Free energy diagrams and corresponding reaction intermediates for NRR via a mixed pathway on V-Cu@GDY.

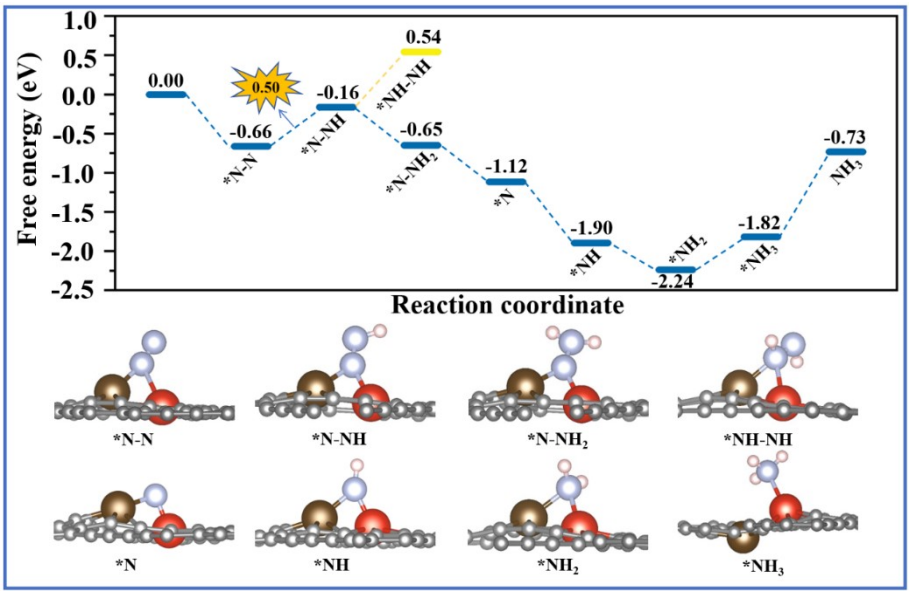

Fig. S22 Free energy diagrams and corresponding reaction intermediates for NRR via a distal pathway on V-Fe@GDY.

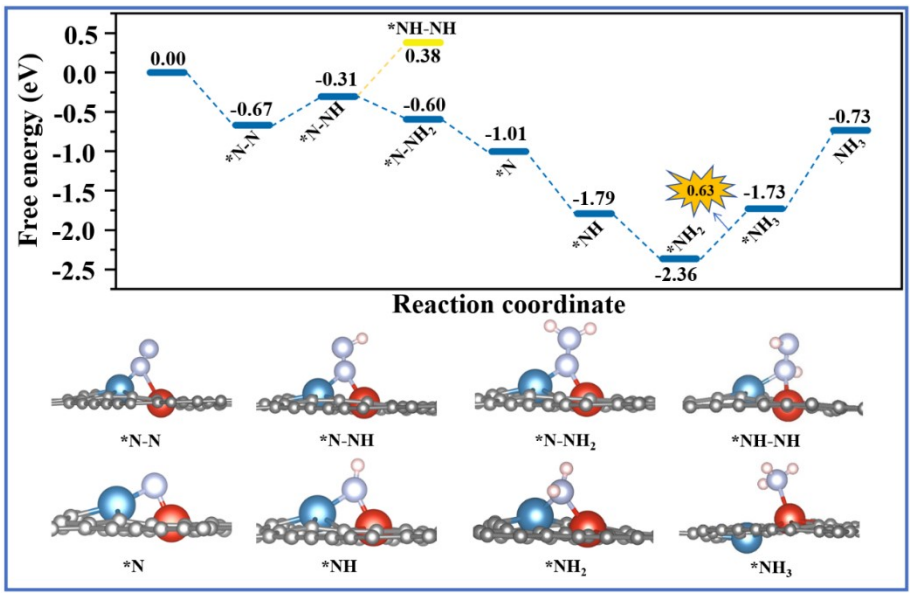

Fig. S23 Free energy diagrams and corresponding reaction intermediates for NRR via a distal pathway on V-Co@GDY.

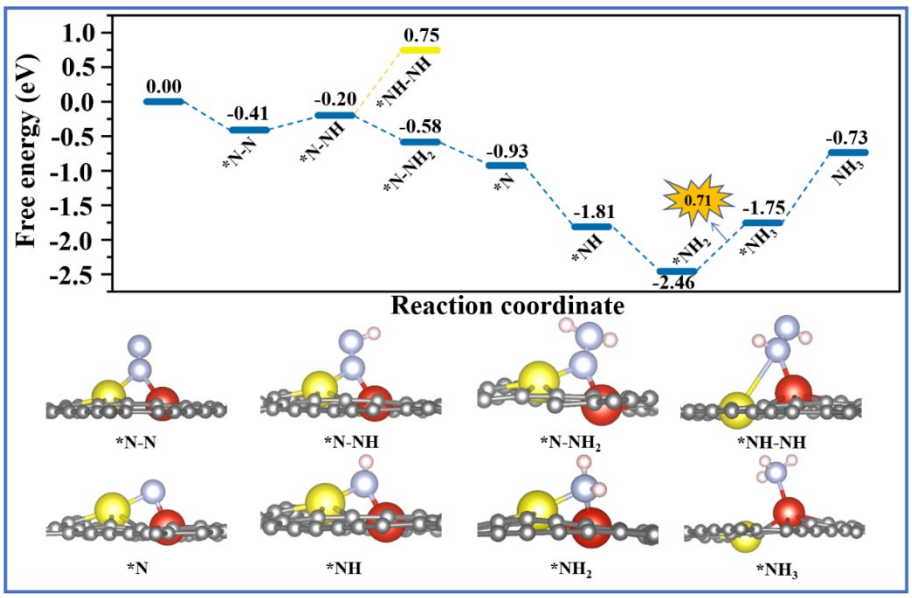

Fig. S24 Free energy diagrams and corresponding reaction intermediates for NRR via a distal pathway on V-Ni@GDY.

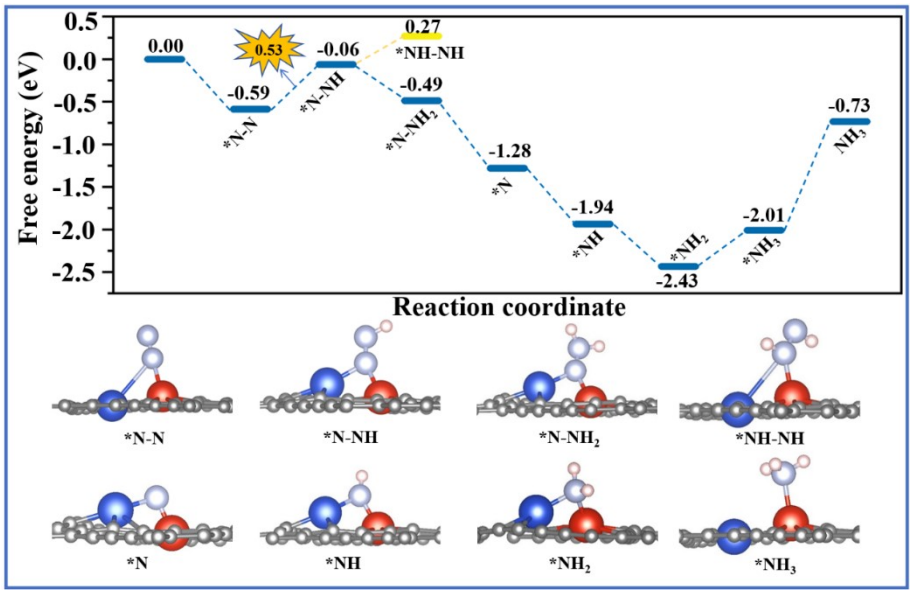

Fig. S25 Free energy diagrams and corresponding reaction intermediates for NRR via a distal pathway on V-Cu@GDY.

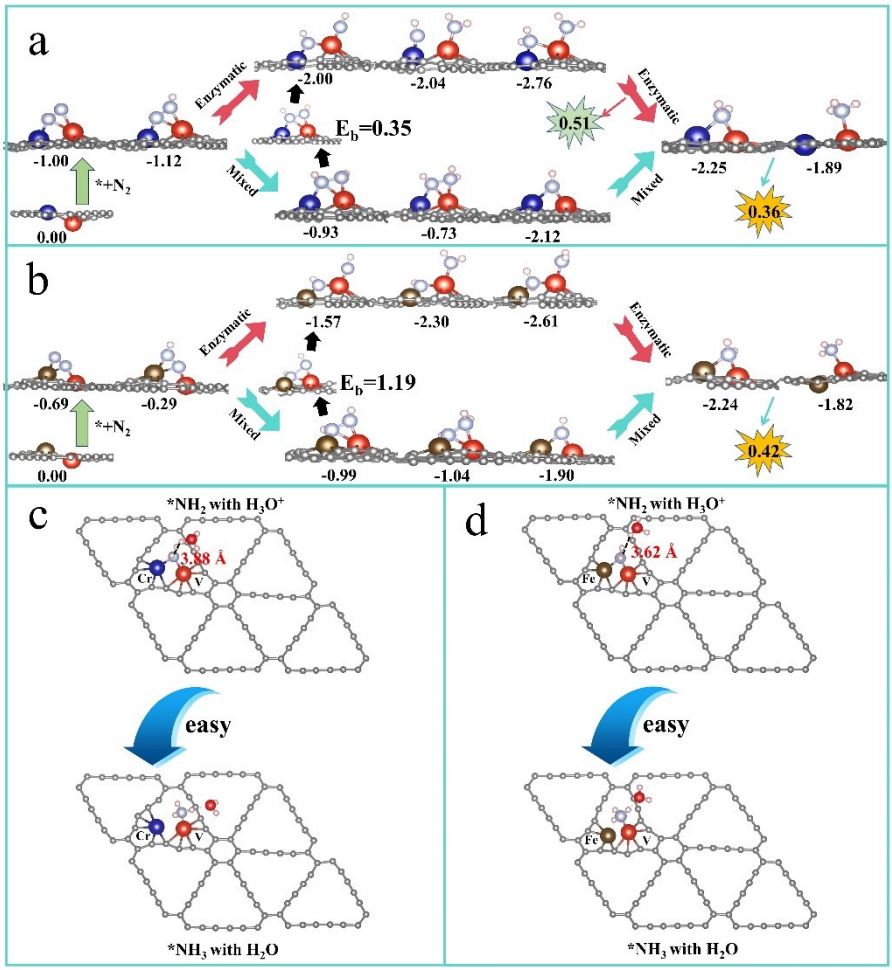

Fig. S26 The intermediates and the free energy changes (in eV) for the NRR on V-Cr@GDY (a) and V-Fe@GDY (b). Easy protonation of $*NH_2$ to $*NH_3$ by H_3O^+ under acidic conditions for V-Cr@GDY (c) and V-Fe@GDY (d). E_b denotes the energy barrier (in eV) for the dissociation of the adsorbed species.

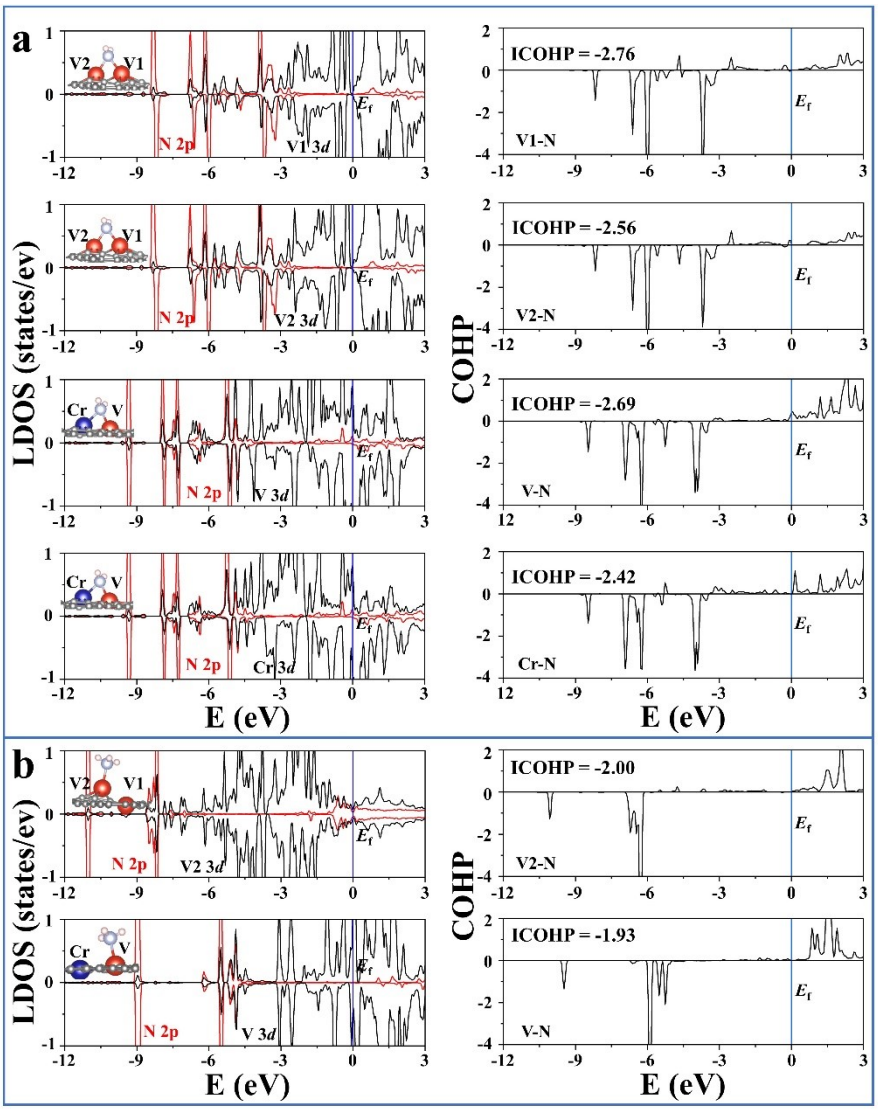

Fig. S27 The LDOS projected on the N atom of the adsorbed NH_2 species and its bonded TM atoms, and the relevant pCOHP and ICOHP (a), and The LDOS projected on the N atom of the adsorbed NH_3 species and its bonded TM atoms, and the relevant pCOHP and ICOHP (b).

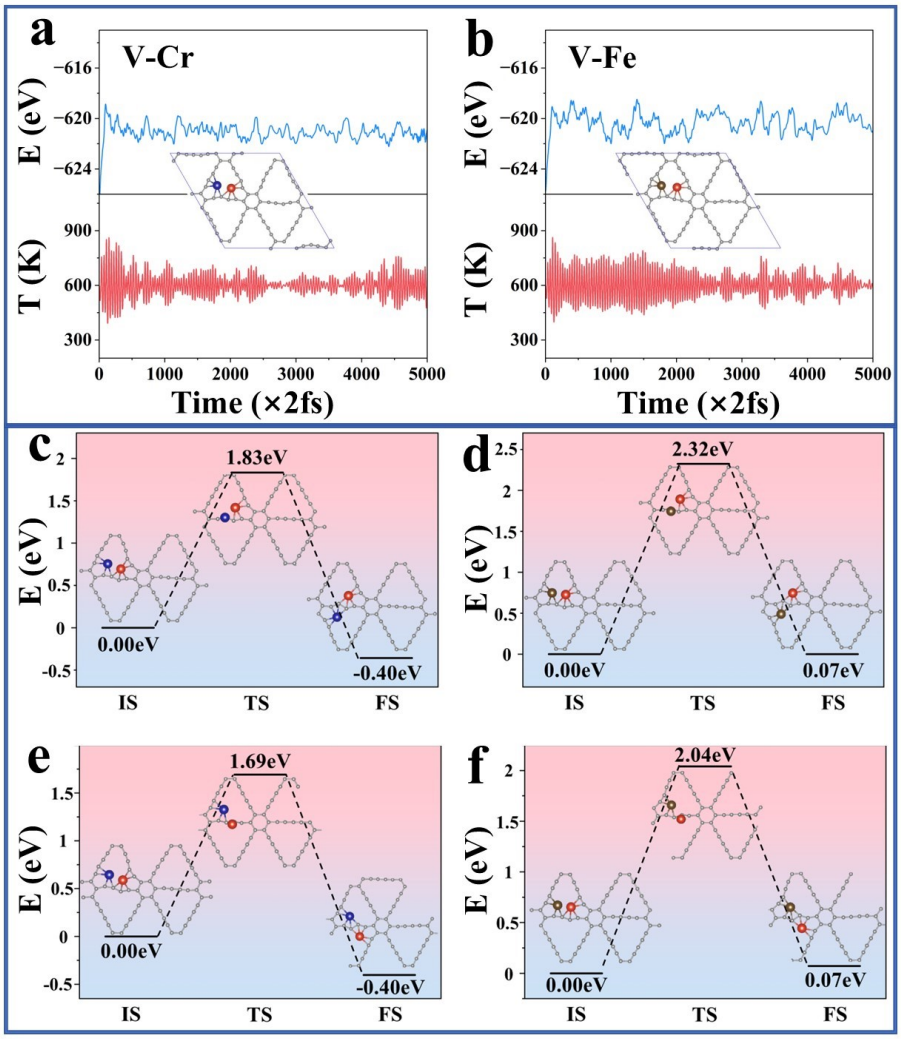

Fig. S28 Energy and temperature fluctuations against the time in AIMD simulations over 10 ps at 600 K for V-Cr@GDY (a), V-Fe@GDY (b). Optimized structures of the initial state (IS), transition state (TS), final state (FS), and the energy barrier for the dissociation of the V-Cr pair in V-Cr@GDY (b-c) and the V-Fe pair in V-Fe@GDY (d-e), leading to the formation of separated single atoms.

Reference

1. X. Guo; J. Gu; S. Lin; S. Zhang; Z. Chen; S. Huang, Tackling the Activity and Selectivity Challenges of Electrocatalysts toward the Nitrogen Reduction Reaction Via Atomically Dispersed Biatom Catalysts, *J. Am. Chem. Soc.*, 2020, ***142***, 5709-5721.

2. W. Zhao; L. Zhang; Q. Luo; Z. Hu; W. Zhang; S. Smith; J. Yang, Single

Mo1(Cr1) Atom on Nitrogen-Doped Graphene Enables Highly Selective Electroreduction of Nitrogen into Ammonia, *ACS Catal.*, 2019, ***9***, 3419-3425.

3. X. Liu; Y. Jiao; Y. Zheng; M. Jaroniec; S.-Z. Qiao, Building up a Picture of the Electrocatalytic Nitrogen Reduction Activity of Transition Metal Single-Atom Catalysts, *J. Am. Chem. Soc.*, 2019, ***141***, 9664-9672.

4. X. Wang; Q. Zhang; W. Hao; C. Fang; J. Zhou; J. Xu, A Novel Porous Graphitic Carbon Nitride (G-C7n3) Substrate: Prediction of Metal-Based Π–D Conjugated Nanosheets toward the Highly Active and Selective Electrocatalytic Nitrogen Reduction Reaction, *J. Mater. Chem. A.*, 2022, ***10***, 15036-15050.

5. Http://Webbook.Nist.Gov/Chemistry/.

6. Z. Feng; Y. Tang; W. Chen; Y. Li; R. Li; Y. Ma; X. Dai, Graphdiyne Coordinated Transition Metals as Single-Atom Catalysts for Nitrogen Fixation, *Phys. Chem. Chem. Phys.*, 2020, ***22***, 9216-9224.